

Modulation of CO adsorption on 4,12,2-graphyne by Fe atom doping and applied electric field

Yu Dong(董煜), Zhi-Gang Shao(邵志刚), Cang-Long Wang(王苍龙), and Lei Yang(杨磊)
Citation: Chin. Phys. B, 2023, 32 (**8**): 087101. DOI: 10.1088/1674-1056/acc935
Journal homepage: http://cpb.iphy.ac.cn; http://iopscience.iop.org/cpb

What follows is a list of articles you may be interested in

Infrared optical absorption of Fröhlich polarons in metal halide perovskites

Yu Cui(崔钰), Xiao-Yi Liu(刘晓逸), Xu-Fei Ma(马旭菲), Jia-Pei Deng(邓加培), Yi-Yan Liu(刘怡言), and Zi-Wu Wang(王子武)
Chin. Phys. B, 2023, 32 (**9**): 097102. DOI: 10.1088/1674-1056/aca7f0

Single crystal growth and electronic structure of Rh-doped $Sr_3Ir_2O_7$

Bingqian Wang(王冰倩), Shuting Peng(彭舒婷), Zhipeng Ou(欧志鹏), Yuchen Wang(王宇晨), Muhammad Waqas, Yang Luo(罗洋), Zhiyuan Wei(魏志远), Linwei Huai(淮琳崴),Jianchang Shen(沈建昌), Yu Miao(缪宇), Xiupeng Sun(孙秀鹏), Yuewei Yin(殷月伟), and Junfeng He(何俊峰)
Chin. Phys. B, 2023, 32 (**8**): 087108. DOI: 10.1088/1674-1056/acd7d5

Atomistic simulations of graphene origami: Dynamics and kinetics

Panpan Zhang(张盼盼), Haihong Jia(贾海洪), Yan-Fang Zhang(张艳芳), and Shixuan Du(杜世萱)
Chin. Phys. B, 2023, 32 (**8**): 087107. DOI: 10.1088/1674-1056/acd527

Topological properties of tetratomic Su-Schrieffer-Heeger chains with hierarchical long-range hopping

Guan-Qiang Li(李冠强), Bo-Han Wang(王博涵), Jing-Yu Tang(唐劲羽), Ping Peng(彭娉), and Liang-Wei Dong(董亮伟)
Chin. Phys. B, 2023, 32 (**7**): 077102. DOI: 10.1088/1674-1056/aca7ef

Electronic states of domain walls in commensurate charge density wave ground state and mosaic phase in 1*T*-TaS_2

Yan Li(李彦), Yao Xiao(肖遥), Qi Zheng(郑琦), Xiao Lin(林晓), Li Huang(黄立), and Hong-Jun Gao(高鸿钧)
Chin. Phys. B, 2023, 32 (**7**): 077101. DOI: 10.1088/1674-1056/accd4f

---

Modulation of CO adsorption on 4,12,2-graphyne by Fe atom doping and applied electric field

Yu Dong(董煜)[1], Zhi-Gang Shao(邵志刚)[1,2,†], Cang-Long Wang(王苍龙)[3,4], and Lei Yang(杨磊)[3,4]

[1] *Guangdong Provincial Key Laboratory of Quantum Engineering and Quantum Materials, Guangdong Engineering Technology Research Center of Efficient Green Energy and Environment Protection Materials, SPTE, South China Normal University, Guangzhou* 510006, *China*

[2] *Guangdong–Hong Kong Joint Laboratory of Quantum Matter, Frontier Research Institute for Physics, South China Normal University, Guangzhou* 510006, *China*

[3] *Institute of Modern Physics, Chinese Academy of Sciences, Lanzhou* 730000, *China*

[4] *School of Nuclear Science and Technology, University of Chinese Academy of Sciences, Beijing* 100049, *China*

(Received 8 February 2023; revised manuscript received 15 March 2023; accepted manuscript online 31 March 2023)

Adsorption characteristics of CO adsorbed on pristine 4,12,2-graphyne (4,12,2-G) and Fe-doped 4,12,2-graphyne (Fe-4,12,2-G) are studied by first-principles calculations. It is shown that CO is only physically adsorbed on pristine 4,12,2-G. Fe atoms can be doped into 4,12,2-G stably and lead to band gap opening. After doping, the interaction between Fe-4,12,2-G and CO is significantly enhanced and chemisorption occurs. The maximum adsorption energy reaches −1.606 eV. Meanwhile, the charge transfer between them increases from 0.009*e* to 0.196*e*. Moreover, the electric field can effectively regulate the adsorption ability of the Fe-4,12,2-G system, which is expected to achieve the capture and release of CO. Our study is helpful to promote applications of two-dimensional carbon materials in gas sensing and to provide new ideas for reversible CO sensor research.

Keywords: CO, Fe-doped 4,12,2-graphyne, applied electric field, first-principles calculations

PACS: 71.15.Mb, 68.43.–h, 68.43.Fg, 73.20.At **DOI:** 10.1088/1674-1056/acc935

1. Introduction

Carbon monoxide (CO) is a toxic gas with colorless and odorless, usually created by the inadequate combustion of carbon compounds, such as thermal power generation and motor vehicle exhaust. The affinity between CO and hemoglobin (Hb) is 250 times higher than that of oxygen, and its separation from Hb is slow.[1] This causes it easy to combine with Hb in the human body to form carboxyhemoglobin, which leads to hypoxic in the body. In severe cases, this can lead to cardiopulmonary dysfunction and brain atrophy, and even death.[2,3] In addition, there is a risk of explosion when the volumetric concentration of CO in air reaches 12.5% to 74.2%.[4] Therefore, it has great significance to explore sensors for efficient detection and adsorption of the CO molecule.

In 2004, graphene has been successfully exfoliated, disproving the understanding that two-dimensional (2D) materials cannot exist freely at finite temperatures, leading to the rise of 2D materials research.[5] Graphene has high carrier mobility (15000 $\mathrm{cm^2/V\cdot s}$), large specific surface area (2630 $\mathrm{m^2/g}$), low resistivity (10^{-6} Ω) and other characteristics, and is suitable for gas sensing.[6–9] Since then, researchers have focused their attention on finding new 2D carbon materials. In recent years, various carbon allotropes have been proposed theoretically and experimentally, including graphdiyne,[10] pentagraphene,[11] net-Y,[12] square graphynes,[13] biphenylene,[14] holey graphyne,[15] and so on. Noticeably, 4,12,2-graphyne (4,12,2-G) is one of the square graphynes, which is proposed by Zhang *et al.*,[13] and 4,12,2-G is a Dirac material composed of 4- and 12-membered rings linkage. Its Fermi surface shows a crescent shape. It has an effective mass of $m = 0.16m_e$, as well as the Fermi velocity varies dramatically from 0.6×10^5 m/s to 5.8×10^5 m/s in different directions, which is close to graphene. Yang *et al.* investigated the electronic and mechanical properties of B- or N-doped 4,12,2-G.[16] It is shown that the doped 4,12,2-G has good electronic and thermal conductivity as well as the B atom doping brings about a giant piezoelectric constant. Moreover, its large size carbon ring can provide more adsorption sites for atoms or functional groups. Therefore, 4,12,2-G is expected to be used in the field of hydrogen storage, lithium-ion battery, gas sensors and new 2D electronic devices.[17,18]

At present, studies on 4,12,2-G have been limited to mechanical and electronic properties and have not addressed the gas adsorption aspects. Therefore, it is essential to research the gas adsorption characteristics of 4,12,2-G and explore its potential as a gas sensing and trapping material. However, similar to graphene, the relatively stable physical and chemical properties of carbon atoms in 4,12,2-G may lead to weak adsorption of CO. The gapless property of 4,12,2-G also limits its application in electronic equipment. Encouragingly, the existing research indicates that the electronic properties of graphene can be changed or even the adsorption performance

†Corresponding author. E-mail: zgshao@scnu.edu.cn

© 2023 Chinese Physical Society and IOP Publishing Ltd

can be improved by introducing defects,[19,20] doping metal atoms,[21–24] modifying functional groups,[25,26] and other means. It is noteworthy that Fe is often selected as a doped atom to improve the adsorption capacity of carbon materials for CO gas.[27–29] Li *et al.* showed that the adsorption energy of Fe-doped net-Y for CO can reach −4.114 eV.[28] Yang *et al.* reported that Fe doping increases the adsorption energy of Stone–Wales graphene (SW-G) for CO from −0.556 eV to −1.588 eV, and it can adsorb up to four CO molecules.[29] In addition, the electric field (E-field) has been found to control the electronic properties of 2D materials.[30,31] By changing the size and direction of the E-field, the effect of controlling gas adsorption or desorption can be achieved.[32–34]

In this work, we investigate the adsorption of CO on pristine 4,12,2-G. Then, effect of the Fe atom as the dopant on the adsorption properties of 4,12,2-G is studied. The adsorption characteristics of CO on 4,12,2-G and Fe-doped 4,12,2-G (Fe-4,12,2-G) are investigated in detail by adsorption energy, total or projected density of states (TDOS or PDOS), charge density difference, total charge density, and Bader charge. Finally, the applied E-field is also considered to study the potential means of CO reversible adsorption. These results provide a theoretical basis for finding potential CO capture materials and achieving reversible adsorption of CO.

2. Model and method

All first-principles calculations in this paper were performed by the Vienna *ab initio* simulation package (VASP).[35,36] The interaction between ion and electron was described by projector augmented wave (PAW) potential.[37] The Perdew–Burke–Ernzerhof (PBE) under the generalized gradient approximation (GGA) was used to describe electron exchange and correlation potential.[38] The cutoff energy was set as 520 eV. All the atomic position optimizations were performed using the conjugate gradient method. The convergence criterion of total energy between two iterations was set at 1×10^{-5} eV. After the structural optimization, the maximum force per atom was less than 0.01 eV/Å. Grimme's DFT-D3 method was used for wan der Waals correction of the system energy.[39] The 2×2 supercell (64 atoms) was constructed and a 15 Å vacuum space was built along the perpendicular substrate direction. The sampling of Brillouin zone was based on Gamma centered Monkhorst–Pack scheme. The $3\times3\times1$, $6\times6\times1$, and $11\times11\times1$ k-meshes were used for structural relaxation, self consistent calculation, and electronic structure calculation, respectively. Bader charge analysis was used to calculate the charge transfer between CO molecule and substrate.[40]

After Fe doping, the stability of Fe-4,12,2-G substrate can be evaluated using the binding energy (E_b) and cohesive energy (E_{coh}). E_b is defined as

$$E_b = E_{\text{Fe-4,12,2-G}} - E_{SV} - E_{Fe}, \tag{1}$$

where $E_{\text{Fe-4,12,2-G}}$ represents the energy of Fe-4,12,2-G, E_{SV} and E_{Fe} represent the energy of Fe-4,12,2-G with single vacancy defect and single Fe atomic energy, respectively. The E_{coh} formula is given as follows:

$$E_{coh} = (E_{\text{Fe-4,12,2-G}} - nE_C - mE_{Fe})/(n+m), \tag{2}$$

where $E_{\text{Fe-4,12,2-G}}$, E_C, and E_{Fe} represent the energies of Fe-4,12,2-G, single C atom, and single Fe atom, respectively; n and m represent the numbers of C and Fe atoms, respectively.

The adsorption energy (E_{ad}) of CO on the surface of pristine 4,12,2-G or Fe-4,12,2-G substrates is calculated by

$$E_{ad} = E_{\text{Sub+CO}} - E_{\text{Sub}} - E_{CO}, \tag{3}$$

where $E_{\text{Sub+CO}}$, E_{Sub}, and E_{CO} represent the total energy of CO adsorbed on substrate surface at stable state, the energy of substrate, and the energy of CO, respectively.

3. Results and discussion

3.1. Structure and electronic properties of 4,12,2-G and Fe-4,12,2-G

Here, 4,12,2-G is a carbon allotrope composed of sp and sp^2 hybridized carbons with square symmetry and a planar group of $P4mm$. Figure 1(a) shows the optimized 4,12,2-G supercell structure. The lattice constants of supercell are $a=b=14.914$ Å. The lengths of l_1, l_2, and l_3 are 1.469 Å, 1.403 Å, and 1.226 Å, respectively, which agree in general with the literature.[13,41] From Fig. 1(b), by analyzing the band structure, the valence and conduction bands of 4,12,2-G form a Dirac cone at the asymmetric point B. Similarly, the density of states (DOS) diagram indicates that there is essentially no occupancy of states at 0 eV, suggesting that 4,12,2-G has semimetallic properties similar to graphene.

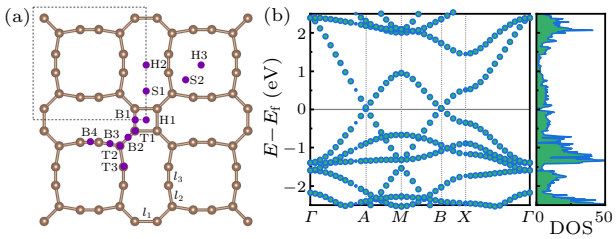


Fig. 1. (a) Structure of 4,12,2-G supercell. (b) Band structure and density of states (DOS) of 4,12,2-G supercell. Brown atoms, purple dots, and black dotted quadrilateral represent carbon atoms, adsorption sites, and unit cell, respectively.

Since the 4,12,2-G supercell has three carbon atoms that are not equivalent, the three different sites (T1, T2, and T3) are considered in the construction of the doping models. However, at T3 site, the structural optimization cannot reach a stable state after Fe atom substitution doping. The possible reason is that Fe doping disrupts the structure originally connected

by sp and sp^2 carbons.[32] Therefore, only the replacement doping of T1 and T2 sites are considered, and both doping concentrations are 1.6%. After the two doping models are fully optimized, the new structure models are obtained, which are named as Fe_1-4,12,2-G and Fe_2-4,12,2-G, respectively, as shown in Fig. 2. According to Fig. 2, we find that there is a significant deformation of structures due to the larger radius of the Fe atom. The Fe atoms move away from 4,12,2-G plane, and the vertical distances from Fe atoms to 4,12,2-G for the two structures are 1.471 Å and 1.630 Å, respectively. At the same time, a corresponding increase in bond length between the Fe atom and three nearest C atoms is observed. Bonds 1, 2, and 3 in the Fe_1-4,12,2-G structure become 1.787 Å, 1.787 Å, and 1.819 Å, respectively. Bonds 4, 5, and 6 in the Fe_2-4,12,2-G structure become 1.791 Å, 1.738 Å, and 1.738 Å, respectively. As listed in Table 1, the results suggest that the E_b values of Fe_1-4,12,2-G and Fe_2-4,12,2-G are −8.573 eV and −10.652 eV, respectively. The E_{coh} values of them are −8.274 eV and −8.271 eV, respectively. These demonstrate that Fe atoms can be doped into 4,12,2-G stably and there exist strong interatomic interactions in the structures.

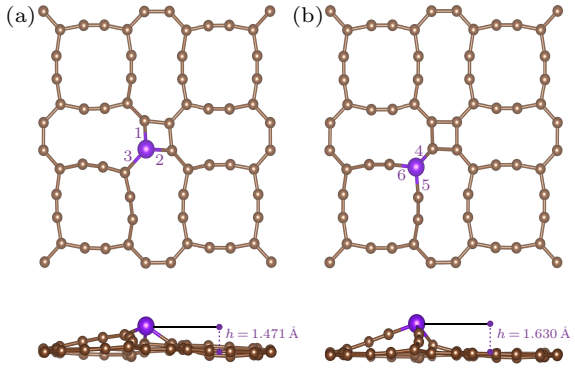


Fig. 2. Top and side views of geometrically optimized structure of (a) Fe_1-4,12,2-G and (b) Fe_2-4,12,2-G. C and Fe atoms are brown and purple, respectively.

Table 1. The binding energy (E_b), cohesive energy (E_{coh}), and band gap (E_{gap}) of 4,12,2-G and Fe-4,12,2-G.

Structure	E_b (eV)	E_{coh} (eV)	E_{gap} (eV)
4,12,2-G	–	−8.383	0
Fe_1-4,12,2-G	−8.573	−8.274	0.123
Fe_2-4,12,2-G	−10.652	−8.271	0.080

Figure 3 shows the unfolding bands and DOS of Fe_1-4,12,2-G and Fe_2-4,12,2-G. In the calculations, the spin polarization is considered. From Figs. 3(a) and 3(b), we find that the doping of Fe disrupts the Dirac cone of 4,12,2-G at the B point and leads to the band gap opening. The corresponding band gaps are 0.123 eV and 0.080 eV, respectively, and the systems have semiconductor characteristic. The spin-up and spin-down DOSs in Figs. 3(c) and 3(d) are basically not different, indicating that the doping of Fe does not cause spin polarization. Meanwhile, the whole systems are nonmagnetic with zero magnetic moment.

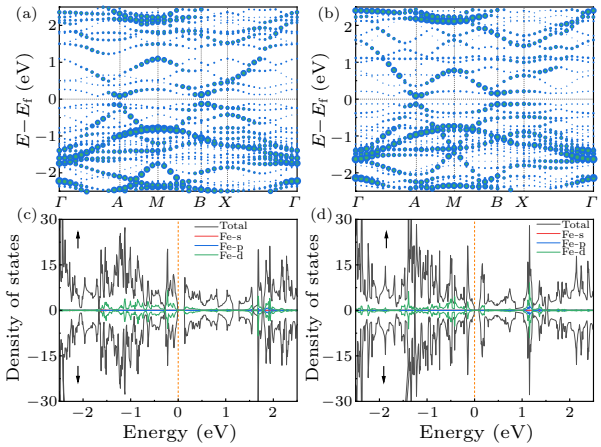


Fig. 3. Band structure and DOS of Fe_1-4,12,2-G [(a), (c)] and Fe_2-4,12,2-G [(b), (d)], with 0 eV representing the Fermi level. The up and down arrows represent spin-up and spin-down DOSs, respectively.

3.2. CO adsorption on pristine 4,12,2-G

Firstly, all possible adsorption sites of CO on 4,12,2-G are considered. As shown in Fig. 1(a), showing the vertex sites (T1, T2, and T3), bridge sites (B1, B2, B3, and B4), hollow sites of carbon rings (H1, H2, and H3), and hollow edge sites of carbon rings (S1 and S2). In addition, different adsorption orientations of CO (vertical and parallel adsorption) are considered. However, due to the asymmetry of CO, vertical adsorption can be further divided into two cases: the C atom of CO pointing downward to the substrate (V_C) and the O atom pointing downward to the substrate (V_O). Secondly, a set of naming rules is formulated to facilitate the representation of the model structure. For example, the vertical adsorption with the C atom pointing downward to substrate at T1 site is named as T1-V_C, and the parallel adsorption at H3 site is named as H3-P. Finally, all possible adsorption configurations are fully optimized. In the supplementary material, Fig. S1 shows all the structures after optimization and Table S1 lists the detailed data for all configurations.

The results in Table S1 show that the E_{ad} values of all configurations are between −0.065 eV and −0.128 eV. H3-P has the largest value, reaching −0.128 eV. The analysis suggests that the C atom of CO prefers pointing to substrate. The degree of adsorption sites tendency is ranked from largest to smallest in the order of vacancy, bridge, and vertex sites. For all adsorption configurations, the bond lengths of CO after adsorption are in the range from 1.143 Å to 1.144 Å, and the adsorption heights are all greater than 2.8 Å. Bader analysis indicates that all charge transfers are positive with a maximum value of 0.009*e*. However, the overall charge transfers are small, which proves that the interaction between CO and 4,12,2-G is weak.

To further analyze the interaction between CO and 4,12,2-G, we select two configurations with the largest E_{ad} value, H3-P and H2-P, and calculate their DOS and total charge density, as shown in Fig. 4. Figures 4(a) and 4(b) show that new peaks

appear around −4.0 eV and 3.0 eV because of the contribution of CO 2p orbital. However, the TDOS of systems does not change near the Fermi level after adsorbing CO. From Figs. 4(c) and 4(d), it can be found that there is no charge density overlap between CO and 4,12,2-G. These further confirm the weak interaction between CO and 4,12,2-G, where only physisorption occurs.

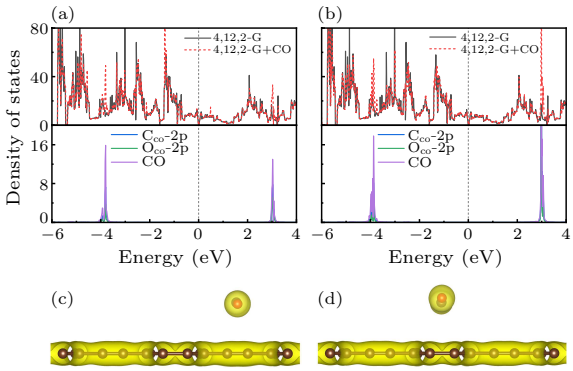


Fig. 4. Total density of states (TDOS), projected density of states (PDOS), and total charge density (0.09 e/Bohr^3) of CO adsorbed on 4,12,2-G: [(a), (c)] H3-P, [(b), (d)] H2-P.

3.3. Effect of single Fe atom doping

In this section, we dope a single Fe atom on 4,12,2-G substrate to explore the effect of Fe doping on the adsorption property of the system. After calculation, Fe-4,12,2-G has two stable configurations, Fe_1-4,12,2-G and Fe_2-4,12,2-G. Due to the introduction of the Fe atom, only the Fe atom is considered as adsorption site, because the Fe atom can interact with either the C or the O atom. As in the case of 4,12,2-G adsorption, the vertical and parallel adsorption configurations of CO are considered. Therefore, there are six adsorption configurations after full optimization, as shown in Fig. 5. According to the previous naming rules, these six configurations are named as Fe-T1-V_C, Fe-T1-V_O, Fe-T1-P, Fe-T2-V_C, Fe-T2-V_O, and Fe-T2-P, respectively. Detailed adsorption information of these configurations is given in Table 2.

Table 2. Adsorption energy (E_{ad}, in eV), adsorption distance (d, in Å), CO bond length (l, in Å), Bader charge transfer (ΔQ, in e) and band gap (E_{gap}, in eV) of different adsorption configurations of Fe-4,12,2-G. Adsorption distance is the distance between the atom closest to the Fe atom in the CO molecule and the Fe atom. The positive and negative values of Bader charge transfer mean that CO gets or loses electrons.

Structure	E_{ad}	d	l	ΔQ	E_{gap}
Fe-T1-V_C	−1.579	1.827	1.162	0.196	0.103
Fe-T1-V_O	−0.320	2.052	1.157	0.061	0.108
Fe-T1-P	−1.579	1.828	1.162	0.196	0.086
Fe-T2-V_C	−1.367	1.832	1.158	0.132	0.085
Fe-T2-V_O	−0.215	2.127	1.154	0.051	0.060
Fe-T2-P	−1.606	1.816	1.160	0.165	0.041

From Fig. 5, it can be found that for the vertical adsorption configurations, the original structural setup (the C or the O atom of CO pointing to the Fe atom) is maintained after full optimization. For parallel adsorption, both Fe-T1-P and Fe-T2-P finally exhibit the C atom closer to the Fe atom, indicating that the Fe atom is more inclined to interact with the C atom. According to Table 2, it is found that for both Fe-4,12,2-G, the V_C and P configurations have higher E_{ad} values (about five times), smaller adsorption distances, longer CO bond lengths, and larger charge transfer (about three times) compared to the V_O configurations. These demonstrate that the V_C and P configurations are more stable than the V_O configuration and have stronger intermolecular interactions between the substrate and CO. The maximum E_{ad} of CO adsorbed on Fe-4,12,2-G is −1.606 eV, which is higher than those of Pt-doped graphene (−1.30 eV),[42] Pd-doped graphene (−1.07 eV),[43] Au_5 clusters supported TiO_2 (−1.37 eV)[44] and Cu-doped MoS_2 (−1.25 eV).[45] And it is close to $H_{4,4,4}$-graphyne (−1.601 eV)[32] as well as Fe-supported $SnSe_2$ (−1.507 eV).[46] A higher E_{ad} value represents higher sensitivity and faster response time. However, it is worth noting that too small or too large values of E_{ad} are not favorable for gas adsorption and desorption, while the range from −2 eV and −1 eV is the most favorable.[32,47] Therefore, compared with the large E_{ad} of Fe-doped net-Y (−4.117 eV),[28] Sb, S co-doped SnO_2 (−5.82 eV)[48] and Co-decorated $MoSe_2$ (−2.419 eV),[49] Fe-4,12,2-G is more suitable for the reversible adsorption of CO. Furthermore, the adsorption distances of V_C and P configurations are found to be less than the sum of the covalent radii of Fe and C (1.91 Å).[50] This suggests that CO can form a chemical bond with Fe-4,12,2-G and they behave as chemisorbed system. Meanwhile, by comparing Fe_1-4,12,2-G and Fe_2-4,12,2-G systems, we find that the Fe_1-4,12,2-G system has greater average E_{ad} and charge transfer. Thus, the Fe_1-4,12,2-G (Fe-T1-V_C) system is more suitable as a sensing material. Compared with the 4,12,2-G (H3-P), doping of the Fe atom leads to an increase in E_{ad} and charge transfer of the adsorption system. Therefore, Fe atom doping is an excellent method to enhance the adsorption capacity of 4,12,2-G for CO.

In order to research the changes in electronic properties of the systems after CO adsorption, the TDOS and PDOS of the adsorbed system are calculated and compared with the unadsorbed system. As shown in Fig. 6, the DOS of Fe-4,12,2-G after adsorbing CO has been changed significantly with a large number of new peaks compared with pristine 4,12,2-G case. According to the PDOS, it can be found that the emerging peaks are mostly caused by the weak hybridization between CO 2p and Fe 3d orbitals. Therefore, it can be concluded that strong interactions occur between the Fe atom and CO, further confirming that Fe doping can lead to the chemisorption of the systems. However, comparing with V_C and P configurations, V_O configuration has a weaker orbital hybridization. From Figs. 6(b) and 6(e), the CO has almost no overlap with the Fe

3d orbital in the range from −2 eV to 0 eV, which may be responsible for the relatively weak adsorption of the V_O configuration. Moreover, we notice a significant change in TDOS after adsorbing CO by Fe-4,12,2-G, especially near the Fermi level. TDOS shifts toward the lower energy level and the band gaps of systems decrease simultaneously (except Fe-T2-V_C). These results are consistent with the data listed in Table 2. The change in band gap will lead to a significant change in conductivity, as conductivity is exponentially related to the negative value of band gap.[51] Therefore, Fe-4,12,2-G substrate is sensitive to CO and adsorption of CO can be converted into electrical signals for easy detection.

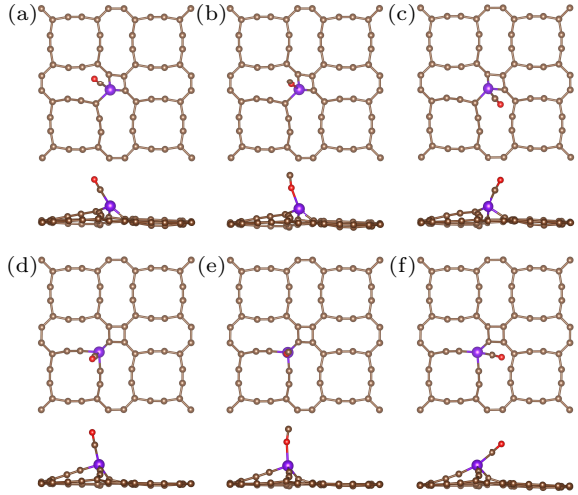


Fig. 5. Top and side views of optimized structure of Fe-4,12,2-G adsorption of CO. (a) Fe-T1-V_C, (b) Fe-T1-V_O, (c) Fe-T1-P, (d) Fe-T2-V_C, (e) Fe-T2-V_O, and (f) Fe-T2-P. Brown, red, and purple atoms represent C, O, and Fe atoms, respectively.

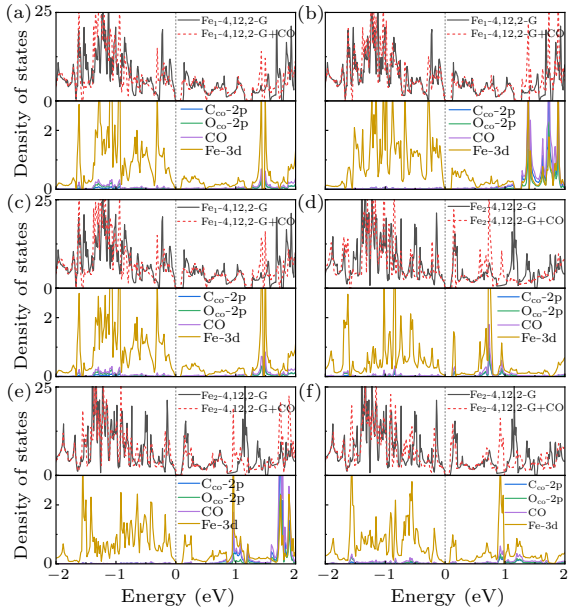


Fig. 6. TDOS and PDOS of (a) Fe-T1-V_C, (b) Fe-T1-V_O, (c) Fe-T1-P, (d) Fe-T2-V_C, (e) Fe-T2-V_O, and (f) Fe-T2-P.

The charge density difference and total charge density after adsorption are shown in Fig. 7. Analysis of charge density difference reveals that electrons are transferred from substrate to CO. Due to Fe atom doping, more electrons loss from substrate and accumulation on CO, which is consistent with Bader analysis. Also, the electron accumulation near the C atom of CO in V_C or P configurations is obviously larger than that of O atom in V_O configuration, which further indicates that the Fe atom interacts more strongly with C atom. Observing the total charge density, there is no charge overlap between CO and substrate in V_O configuration at the isosurface of 0.09 e/Bohr^3, suggesting that the interaction between them is weaker, but still stronger than pristine 4,12,2-G. Therefore, the interaction between Fe-4,12,2-G and CO is stronger and is chemisorbed.

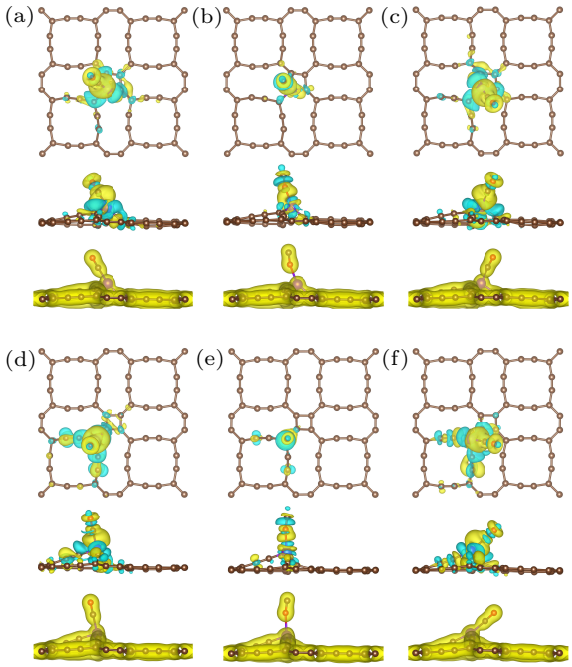


Fig. 7. The charge density difference (0.001 e/Bohr^3) and total charge density (0.09 e/Bohr^3) of (a) Fe-T1-V_C, (b) Fe-T1-V_O, (c) Fe-T1-P, (d) Fe-T2-V_C, (e) Fe-T2-V_O and (f) Fe-T2-P. Yellow represents the accumulation of charge and cyan represents the loss of charge.

3.4. Effect of applied electric field

In this section, we explore the adsorption of CO on 4,12,2-G and Fe-4,12,2-G in the presence of E-field. Based on previous detailed studies, H3-P and Fe-T1-V_C configurations are selected as the research objects. As shown in Fig. 8, the charge transfers for both the configurations under E-field are labeled. Under the positive (negative) E-field, the transfer of electrons in the 4,12,2-G (Fe-4,12,2-G) system works from the substrate to CO. In addition, the detailed calculation data of this section are listed in Table S2.

Figures 9(a) and 9(b) show the curves of adsorption distance and CO bond length of 4,12,2-G and Fe-4,12,2-G systems with E-field. It is noticed that the adsorption distances of 4,12,2-G or Fe-4,12,2-G decrease gradually in the E-field from −0.8 eV/Å to 0.8 eV/Å. The CO bond length of Fe-4,12,2-G changes from 1.148 Å to 1.179 Å. However, the CO bond length of 4,12,2-G changes insignificantly. These phenomena

suggest that the E-field has a significant modulating effect on the structure of the Fe-4,12,2-G system.

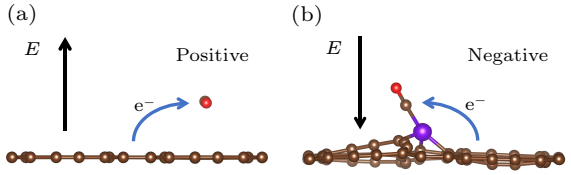


Fig. 8. Charge transfer under applied electric field: (a) 4,12,2-G, (b) Fe-4,12,2-G.

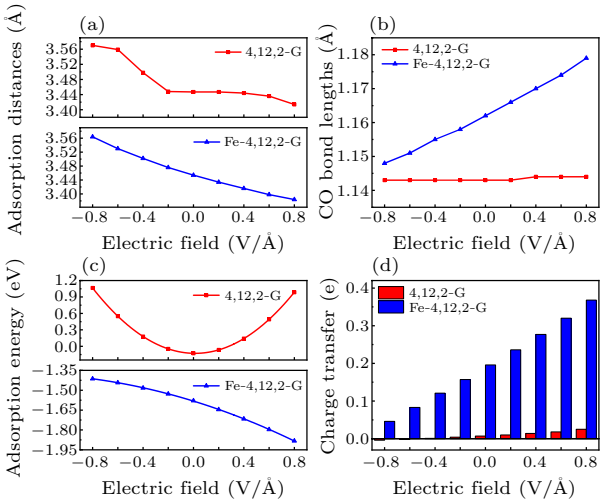


Fig. 9. Effects of electric field change on CO adsorption on 4,12,2-G and Fe-4,12,2-G: (a) adsorption distances, (b) CO bond lengths, (c) adsorption energy, and (d) charge transfer.

Figure 9(c) represents the E_{ad} value and fitting curve with different E-fields. Remarkably, we find that the relationship between E_{ad} value and E-field can be expressed as a quadratic function. This can be explained as the energy stability of the system caused by the induced dipole moment under the applied E-field, namely the second-order Stark effect.[52,53] In addition, it can be observed that the E_{ad} value of the 4,12,2-G system decreases with increasing E-field strength, independent of the direction of E-field. This is similar to the results of Zhang *et al.*[34] Surprisingly, the E_{ad} value is positive when E-field strength is larger than 0.2 V/Å, suggesting that the adsorption may not exist. This behavior may be caused by the difference between the dipole moment of CO and the direction of E-field.[54–56] Regardless of the positive or negative E-field, the intrinsic dipole moment of the parallel adsorbed CO is always perpendicular to the E-field, resulting in weaker adsorption. In contrast to the 4,12,2-G system, the E_{ad} of the Fe-4,12,2-G system increases with the enhancement of positive E-field. When E-field strength is increased from 0 V/Å to 0.8 V/Å, the value of E_{ad} increases from −1.579 eV to −1.882 eV. However, when E-field is increased from 0 V/Å to −0.8 V/Å, the value of E_{ad} decreases from −1.579 eV to −1.414 eV. This is due to the fact that Fe atom doping causes the substrate to have a dipole moment and plays a major role. Under a positive E-field, the dipole moment of the substrate is in the same direction as the E-field, and the E_{ad} is enhanced.[56] On the contrary, under negative E-field, the two directions are opposite and the E_{ad} is weakened. Therefore, the interaction between CO and 4,12,2-G is weakened due to the E-field. The positive (or negative) E-field can enhance (or weaken) the adsorption of the Fe-4,12,2-G system for reversible adsorption.

The Bader analysis and charge density difference can further demonstrate the charge distribution under the applied E-field. For the 4,12,2-G system, electrons move from CO to 4,12,2-G only when the E-field is less than −0.4 V/Å (Fig. 9(d)). However, when the E-field is −0.4 V/Å, the direction of charge movement is reversed and CO acts as an electron acceptor. After that, the charge on CO increases with the increase of E-field. The charge transfer reaches a maximum (0.025e) at 0.8 V/Å. Compared with the 4,12,2-G system, CO has been acting as an electron acceptor in the Fe-4,12,2-G system due to the introduction of Fe (C and O are more electronegative than Fe). It can be found that with the E-field changing from −0.8 V/Å to 0.8 V/Å, the charge transfer from Fe-4,12,2-G to CO increases gradually from 0.046e to 0.368e. Obviously, Fe-4,12,2-G is more responsive to the change of E-field. From Fig. S2, the charge density difference more intuitively reflects the effect of E-field on charge transfer. It is visualized that as the E-field is increasing from −0.8 V/Å to 0.8 V/Å, the yellow region around CO gradually increases and there are more electrons in accumulation. It indicates that the electrons transfer to CO, which is consistent with Fig. 9(d). Especially, for the Fe-4,12,2-G system, the yellow region between Fe and C (CO) atoms increases significantly, further indicating that the interaction between CO and the Fe atom is enhanced by a positive E-field and a stable chemical bond is formed between them.

4. Conclusions

In summary, adsorption of CO on 4,12,2-G and Fe-4,12,2-G has been systematically investigated by first-principles calculations. Our results indicate that the adsorption energy of CO molecules on 4,12,2-G is −0.128 eV and behaves as physical adsorption. Doping of Fe atoms changes the structure of 4,12,2-G and leads to the band gap opening, and the transformation of systems from semimetal to semiconductor. After doping, the adsorption distance between CO and substrate is significantly reduced, while the adsorption energy, CO bond length, and charge transfer are correspondingly increased. Especially, the adsorption energy and charge transfer are 12 and 28 times higher than the original ones, respectively. The observation of total charge density and DOS reveals that there is a significant overlap of electron clouds between CO and Fe-4,12,2-G. The CO 2p orbital overlaps with

Fe 3d orbital, and the system exhibits chemisorption. Meanwhile, along with the adsorption of CO, the band gap of systems changes, leading to a change in the system conductivity and an increase in the sensing sensitivity. Moreover, the present study reveals that the existence of E-field has a significant effect on adsorption systems. For the 4,12,2-G system, the coupling of E-field to the CO dipole moment of the system inhibits the adsorption capacity and is even completely desorbed. For the Fe-4,12,2-G system, the coupling of substrate dipole moment to the positive E-field further increases the adsorption energy and charge transfer. On the contrary, in the negative E-field, the substrate dipole moment is opposite to the direction of E-field, resulting in a weakened adsorption capacity. In a word, Fe-4,12,2-G is a potential CO sensing material with excellent adsorption capacity and high sensitivity.

Acknowledgement

Project supported by the National Natural Science Foundation of China (Grant No. 52072132).

References

[1] Rose J J, Wang L, Xu Q, McTiernan C F, Shiva S, Tejero J and Gladwin M T 2017 *Am. J. Respir. Crit. Care Med.* **195** 596
[2] Hampson N B and Bodwin D 2013 *J. Emerg. Med.* **44** 625
[3] Li F, Chan H C O, Liu S, Jia H, Li H, Hu Y, Wang Z and Huang W 2015 *Forensic Sci. Int.* **253** 112
[4] Su H C and Myung N V 2019 *Electroanalysis* **31** 437
[5] Novoselov K S, Geim A K, Morozov S V, Jiang D, Zhang Y, Dubonos S V, Gregorieva I V and Firsov A A 2004 *Science* **306** 666
[6] Basu S and Bhattacharyya P 2012 *Sens. Actuator B Chem.* **173** 1
[7] Schedin F, Geim A K, Morozov S V, Hill E W, Blake P, Katsnelson M I and Novoselov K S 2007 *Nat. Mater.* **6** 652
[8] Leenaerts O, Partoens B and Peeters F 2008 *Phys. Rev. B* **77** 125416
[9] Yang D, Yang N, Ni J, Xiao J, Jiang J, Liang Q, Ren T and Chen X 2017 *Mater. Des.* **119** 397
[10] Li G, Li Y, Liu H, Guo Y, Li Y and Zhu D 2010 *Chem. Commun.* **46** 3256
[11] Zhang S, Zhou J, Wang Q, Chen X, Kawazoe Y and Jena P 2015 *Proc. Natl. Acad. Sci. USA* **112** 2372
[12] Liu M, Liu M, She L, Zha Z, Pan J, Li S, Li T, He Y, Cai Z, Wang J, Zheng Y, Qiu X and Zhong D 2017 *Nat. Commun.* **8** 14924
[13] Zhang L, Wang Z, Wang Z M, Du S, Gao H J and Liu F 2015 *J. Phys. Chem. Lett.* **6** 2959
[14] Fan Q, Yan L, Tripp M W, Krejčí O, Dimosthenous S, Kachel S R, Chen M, Foster A S, Koert U, Liljeroth P and Gottfried J M 2021 *Science* **372** 852
[15] Liu X, Cho S M, Lin S, Chen Z, Choi W, Kim Y M, Yun E, Baek E H, Ryu D H and Lee H 2022 *Matter* **5** 2306
[16] Yang D C, Tian Z W, Chen Y K, Eglitis R I, Zhang H X and Jia R 2020 *Appl. Surf. Sci.* **499** 143800
[17] Dwivedi S 2022 *Int. J. Hydrog. Energy* **47** 41848
[18] Huang C, Li Y, Wang N, Xue Y, Zuo Z, Liu H and Li Y 2018 *Chem. Rev.* **118** 7744
[19] Zhang H, Lee J Y and Liu H 2021 *J. Phys. Chem. C* **125** 10948
[20] Rafique M, Shuai Y, Tan H P and Hassan M 2017 *Chin. Phys. B* **26** 056301
[21] Gao X, Zhou Q, Wang J, Xu L and Zeng W 2020 *Appl. Surf. Sci.* **517** 146180
[22] Zhao D, Fan X, Luo Z, An Y and Hu Y 2018 *Phys. Lett. A* **382** 2965
[23] Lakshmy S, Kundu A, Kalarikkal N and Chakraborty B 2023 *J. Phys. D: Appl. Phys.* **56** 055402
[24] Liu X J, Cao W Q, Huang Z H, Yuan J, Fang X Y and Cao M S 2015 *Chin. Phys. Lett.* **32** 036802
[25] Choi Y R, Yoon Y G, Choi K S, Kang J H, Shim Y S, Kim Y H, Chang H J, Lee J H, Park C R, Kim S Y and Jang H W 2015 *Carbon* **91** 178
[26] Song M, Chen Y, Liu X, Xu W, Zhao Y, Zhang M and Zhang C 2020 *Phys. Lett. A* **384** 126332
[27] Zhang C P, Li B and Shao Z G 2019 *Appl. Surf. Sci.* **469** 641
[28] Li B, Shao Z G and Fen Y T 2021 *Phys. Chem. Chem. Phys.* **23** 12771
[29] Yang S, Qian X, Xu H, Xiong J, Wang Z and Gu H 2021 *Physica E* **128** 114603
[30] Son Y W, Cohen M L and Louie S G 2006 *Nature* **444** 347
[31] Ni Z, Liu Q, Tang K, Zheng J, Zhou J, Qin R, Gao Z, Yu D and Lu J 2012 *Nano Lett.* **12** 113
[32] Li H B, Feng Y T, Shao Z G, Wang C L and Yang L 2022 *Appl. Surf. Sci.* **586** 152749
[33] Yang S, Lei G, Xu H, Xu B, Li H, Lan Z, Wang Z and Gu H 2019 *Appl. Surf. Sci.* **480** 205
[34] Zhang T, Sun H, Wang F, Zhang W, Ma J, Tang S, Gong H and Zhang J 2018 *Appl. Surf. Sci.* **427** 1019
[35] Kresse G and Furthmüller J 1996 *Phys. Rev. B* **54** 11169
[36] Kresse G and Furthmüller J 1996 *Comput. Mater. Sci.* **6** 15
[37] Kresse G and Joubert D 1999 *Phys. Rev. B* **59** 1758
[38] Perdew J P, Burke K and Ernzerhof M 1996 *Phys. Rev. Lett.* **77** 3865
[39] Grimme S, Antony J, Ehrlich S and Krieg H 2010 *J. Chem. Phys.* **132** 154104
[40] Henkelman G, Arnaldsson A and Jónsson H 2006 *Comput. Mater. Sci.* **36** 354
[41] Yang D C, Tian Z W, Chen Y K, Eglitis R I, Zhang H X and Jia R 2020 *Appl. Surf. Sci.* **499** 143800
[42] Wanno B and Tabtimsai C 2014 *Superlattices Microstruct.* **67** 110
[43] Zhang J N, Ma L, Zhang M and Zhang J M 2020 *Physica E* **118** 113879
[44] Wang Y J, Wang C Y and Eang S Y 2011 *Chin. Phys. B* **20** 036801
[45] Sharma A, Anu, Khan M S, Husain M, Khan M S and Srivastava A 2018 *IEEE Sens. J.* **18** 2853
[46] Pang D, Shi P, Lin L, Xie K, Deng C and Zhang Z 2023 *Phys. Chem. Chem. Phys.* **25** 6626
[47] Obodo K O, Ouma C N M, Obodo J T, Gebreyesus G, Rai D P, Ukpong A M and Bouhafs B 2021 *Nanotechnology* **32** 355502
[48] Li W, Ding C, Li J, Ren Q, Bai G and Xu J 2020 *Appl. Surf. Sci.* **502** 144140
[49] Wang J, Hou Y, Zhang X, Xu Z, Liu G, Hussain S and Qiao G 2023 *Appl. Surf. Sci.* **610** 155399
[50] Pyykkö P and Atsumi M 2009 *Chem. Eur. J.* **15** 186
[51] Ma L, Zhang J M, Xu K W and Ji V 2015 *Appl. Surf. Sci.* **343** 121
[52] Hyman M P and Medlin J W 2005 *J. Phys. Chem. B* **109** 6304
[53] Che F, Gray J T, Ha S and McEwen J S 2015 *J. Catal.* **332** 187
[54] Ma S, Yuan D, Jiao Z, Wang T and Dai X 2017 *J. Phys. Chem. C* **121** 24077
[55] Lin K Y, Nachimuthu S, Nguyen M T, Mizuta H and Jiang J C 2019 *J. Phys. Chem. C* **123** 30373
[56] Yeh C H, Chen Y T and Hsieh D W 2021 *RSC Adv.* **11** 33276